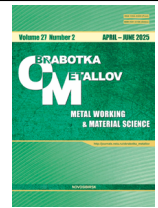# Obrabotka metallov –
Metal Working and Material Science

Journal homepage: http://journals.nstu.ru/obrabotka_metallov

Effect of cold radial forging on structure, texture and mechanical properties of lightweight austenitic steel

Dmitrii Panov [1, a, *], Ruslan Chernichenko [1, b], Stanislav Naumov [1, s], Egor Kudryavtsev [1, d], Gennady Salishchev [1, e], Alexey Pertsev [2, f]

[1] Belgorod National Research University, 85 Pobedy Str., Belgorod, 308015, Russian Federation

[2] Department Chief Metallurgist, Perm Scientific-Research Technological Institute, 41 Geroev Khasana Str., Perm, 614990, Russian Federation

[a] https://orcid.org/0000-0002-8971-1268, ✉ dimmak-panov@mail.ru; [b] https://orcid.org/0000-0002-8619-0700, ✉ rus.chernichenko@mail.ru;
[c] https://orcid.org/0000-0002-4084-8861, ✉ NaumovStanislav@yandex.ru; [d] https://orcid.org/0000-0003-1113-0807, ✉ kudryavtsev@bsuedu.ru;
[e] https://orcid.org/0000-0002-0815-3525, ✉ salishchev_g@bsuedu.ru; [f] https://orcid.org/0009-0009-0771-9345, ✉ perets_87@mail.ru

ARTICLE INFO

ABSTRACT

Introduction. Lightweight austenitic steels, exhibiting high mechanical properties combined with cost-effective alloying and low density, are promising materials for automotive and airspace industries. **The purpose of this work** is to study the evolution of the structure and properties of *Fe-21Mn-6Al-1C* lightweight austenitic steel after cold radial forging (*CRF*) under various modes. **Methods.** Microstructural studies were performed using transmission and scanning electron microscopy (*TEM*) on *JEOL JEM-2100* and *FEI Nova NanoSEM 450* microscopes, respectively. Microhardness was determined in the cross-section using a *Wolpert 402MVD* microhardness tester with a load of 200 g and a dwell time of 15 s. Uniaxial tension testing of samples cut from the edge and center was performed on an *Instron 5882* machine at room temperature and a strain rate of 1×10^{-3} s^{-1}. **Results and discussion**. The stages of structure formation were determined: after deformation (ε) of up to 20 %, the formation of deformation microbands in the center and parallel deformation microbands at the rod edge takes place; after $\varepsilon = 40$–60 %, the formation of single mechanical twins in the center and packets of twins/lamellas at the edge occurs; after $\varepsilon = 80$ %, the intensive twinning in the center and formation of a fragmented structure at the edge takes place. Increasing the degree of *CRF* leads to the development of a sharp two-component axial texture <111>// rod axis (*RA*) and <100>//*RA* in the center, which is blurred towards the edge. At the edge of the rod, a shear texture $B/\bar{B}$ is observed after *CRF* with $\varepsilon = 40$ % and higher. After *CRF* with $\varepsilon = 20$ %, the material in the center of the rod exhibits higher strength and hardness and lower ductility compared to the edge. Further *CRF* is accompanied by a change in this strength/hardness and ductility ratio between the center and the edge of the rod to the opposite. Thus, *CRF* is a promising method for producing industrial blanks from lightweight austenitic steels.

Introduction

Lightweight austenitic steels (*LWASs*) have recently attracted increasing attention due to their cost-effective alloying, high strength, ductility, and impact toughness [1–4]. The presence of such elements as manganese, carbon, aluminum, and silicon in *LWASs* decreases the density of the material by up to 18 % compared to traditional steels, which further increases the attractiveness of these materials for automotive and airspace industries. However, *LWASs* require the development of new approaches to fabrication and processing, which is determined by the emergence of a new deformation mechanism - the formation

* Corresponding author
Panov Dmitrii D., Ph.D. (Engineering),
Belgorod National Research University,
85 Pobedy Str.,
308015, Belgorod, Russian Federation
Tel.: +7 4722 30-12-11, **e-mail:** dimmak-panov@mail.ru

of deformation microbands (microband-induced plasticity - *MBIP*) [5, 6], on the one hand. On the other hand, during heating of such materials, an aging phenomenon is observed - precipitation of nanoparticles of κ'- carbides, B2- and/or DO_3- phases [7–10], which is accompanied by significant strengthening and a decrease in ductility.

The structure formation of *LWASs* during cold plastic deformation has currently been studied mainly in cold rolling and uniaxial tension [5, 11–13]. The high stacking fault energy (*SFE*) of such materials (60-120 mJ/m^2) at room temperature determines dislocation slip as the main mechanism of plastic deformation [1]. In this case, the phenomenon of short-range ordering due to alloying with aluminum causes deformation due to the formation of microbands in the {111} planes. It has been established that at early stages of deformation (ε up to 10 %) in *Fe-28Mn-10Al-1C* steel a *Taylor* lattice is formed from dislocation microbands of two different systems [5]. With an increase in the degree of deformation, an accumulation of misorientation occurs between the domains of the *Taylor* lattice, which after ε = 60 % leads to the fragmentation of initial austenitic grains.

Meanwhile, there are other methods of severe plastic deformation without cracking, for example, radial forging [14, 15]. Recently, it has been shown that cold radial forging with high degrees of deformation (to 90 %) resulted in the development of heterogeneous structures in austenitic alloys [16–18]. This phenomenon is caused by the non-uniform distribution of the operating stresses and temperatures across the rod cross-section during deformation processing. Thus, high compressive stresses act in the rod edge, and moderate tensile stresses are predicted in the rod core. In addition, due to external water cooling and deformation-induced internal heating of the rod core, a gradient in the temperature distribution across the cross-section is observed. However, the effect of radial forging on the microstructure and mechanical properties of *LWASs* requires separate consideration.

The purpose of this work is to study the evolution of the microstructure, texture, and mechanical properties of the lightweight austenitic steel *Fe-21Mn-6Al-1C* subjected to cold radial forging. ***To achieve this purpose, the following objectives were addressed***:

- to determine the effect of the degree of deformation on the microstructure in the cross-section of the rod;

– to determine the effect of the degree of deformation on the texture in the cross-section of the rod;

– to study the distribution of microhardness in the cross-section of the rod after cold radial forging (*CRF*);

– to determine the effect of the degree of deformation on the mechanical properties of the material after cold radial forging (*CRF*).

Methods

The object of the study was the lightweight austenitic steel *Fe-21Mn-6Al-1C* in the form of rods with an experimental composition including the following components (wt. %): *19.76 % Mn; 6.08 % Al; 0.25 % Ni; 1.01 % C; 0.004 % P; 0.004 % S; Fe* – balance. The initial ingot was obtained from pure materials by vacuum arc melting. Then, the ingot was subjected to hot working in the temperature range of 900–1,100 °C in order to obtain a rod for subsequent cold radial forging. The rod with a diameter of 39 mm was annealed (austenitized) at 1,050 °C for 2 hours with cooling in water. The rod was subsequently cold radially forged using a radial forging machine with a feed rate of 180 mm/min, a striker frequency of 1,000 strokes per minute (spm), and a rotation speed of 25 rpm. During the deformation process, the rod was water cooled. Four stages of forging were carried out: from ~39 mm to ~34 mm, from ~34 mm to ~29 mm, from ~29 mm to ~24 mm, from ~24 mm to ~18 mm, which amounted to ~20 %, ~40 %, ~60 % and ~80 % of the relative deformation, respectively.

The microstructure was examined in the cross section of the rod on thin foils using scanning electron microscopy (*SEM*) and transmission electron microscopy (*TEM*). Specimens 0.3 mm thick were cut using an electrical discharge machine, thinned to 0.1 mm by grinding on abrasive paper and polished in an electrolyte (electrolyte composition: 5 % perchloric acid, 35 % butanol and 60 % methanol) at room

temperature and a voltage of 26 V. *SEM* studies were carried out using a *FEI Nova NanoSEM 450* scanning electron microscope equipped with an *EDAX Hikari electron backscatter diffraction (EBSD)* camera. *EBSD* analysis was performed with a scanning step of 100 nm. For subsequent texture evaluation, only results with a confidence index *(CI)* of more than 0.1 were used, which improved the quality of the *EBSD* analysis results. *TEM* studies were conducted using a *JEOL JEM-2100* microscope at an accelerating voltage of 200 kV.

Vickers microhardness was determined using a *Wolpert 402MVD* hardness tester using a diamond pyramid with an angle of 136° at the apex. The tests were carried out in the cross section of the rods along two mutually perpendicular diameters. The indentation step was calculated for each diameter separately, taking into account 70 measurements per diameter. The load applied to the indenter was 200 g with an indentation time of 15 s. The results of microhardness measurements obtained along two mutually perpendicular diameters in the cross-section of the specimen were averaged.

Tensile tests were carried out at room temperature and a strain rate of 1×10^{-3} s^{-1} using an *Instron 5882* electromechanical testing machine. Specimens were cut from the center and subsurface layers of the rod in the axial direction. The dimensions of the gauge of the specimen were $6 \times 3 \times 1.5$ mm^3. Mechanical properties (yield strength, ultimate tensile strength, elongation to failure) were determined according to *GOST 1497-23*. The elongation of specimens during testing was measured using the *VIC-3D* system. For this purpose, one of the side surfaces of the specimens was first coated with white paint, followed by the application of small drops of black paint. The *VIC 2D* program was used to process the obtained data. At least two specimens were tested at each point.

Results and discussion

Austenitization of *Fe-21Mn-6Al-1C* steel produced a fully austenitic, face-centered cubic (*FCC*) structure (Fig. 1, *a*). The microstructure, phase, and chemical composition were uniform across the cross section of the rod. The average size of austenite grains was 150 μm (Fig. 1, *b*), but annealing twins further fragmented the grains, reducing the average distance between high-angle grain boundaries to 55 μm. The fraction of twinned boundaries (*Σ3*) did not exceed 34 %. The direct and reverse pole figures show a weak two-component axial texture <111>// rod axis (*RA*) and <100>//*RA* (Fig. 1, *c* and *d*).

The results of the study of the microstructure evolution during the *CRF* process are shown in Fig. 2. 20 % *CRF* causes microbanding along various systems. It should be noted that in the direction from the center to the edge, the deformation microbands become more pronounced (Fig. 2, *a₁* and *a₂*). According to diffraction
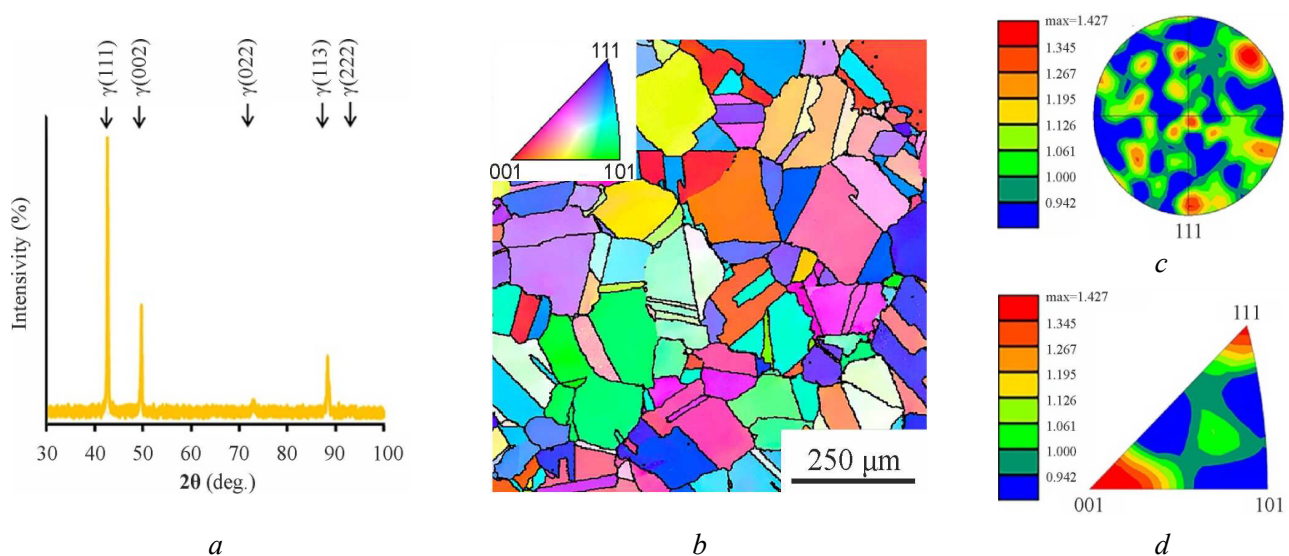

Fig. 1. X-ray diffraction pattern (*a*), grain misorientation map (*b*), direct pole figure (*c*), and inverse pole figure (*d*) of the *Fe-21Mn-6Al-1C steel* in the initial state

analysis, the misorientation between adjacent regions separated by microbands is negligible (<2°). With an increase in the *CRF* reduction to 40 %, mechanical twins appear (Fig. 2, b_1 and b_2). Microdiffraction and *EBSD* analysis indicated that the mechanical twins are located in the {111} planes and are misoriented by approximately 60° relative to the parent austenite (Σ**3** boundary). In this case, parallel primary mechanical twins of one plane set meet in the center of the rod (Fig. 2, b_1), and packets of parallel mechanical twins are formed at the edge of the rod (Fig. 2, b_2). A further increase in the *CRF* reduction to 60 % is accompanied by the development of mechanical twinning in secondary systems in the center of the rod (Fig. 2, c_1). Towards the edge of the rod, a pronounced lamellar structure is observed to form, resulting from mechanical twinning on a single system (Fig. 2, c_2). In addition, shear bands are formed across the twin lamellas (Fig. 2, c_2).

After 80 % *CRF*, an increase in the number of twins in the center of the rod is detected (Fig. 2, d_1). In turn, at the edge of the rod, the structure is fragmented due to the formation of shear bands in the original lamellar microstructure (Fig. 2, d_2).
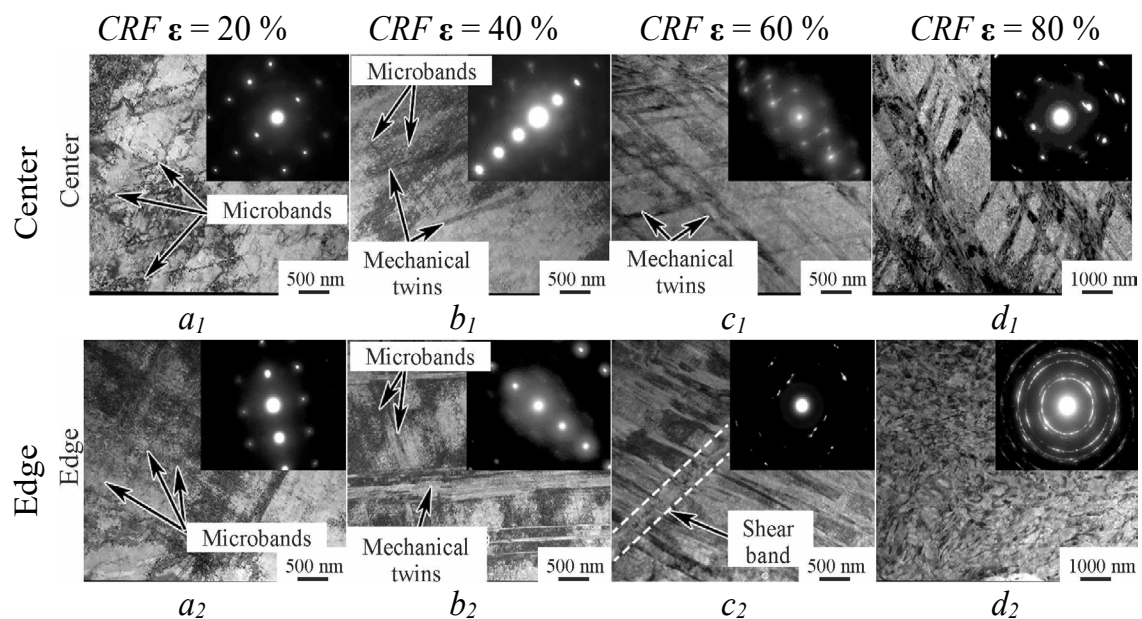

Fig. 2. Fine structure of the *Fe-21Mn-6Al-1C* steel after *CRF* with ε = 20% (a_1, a_2), ε = 40% (b_1, b_2), ε = 60% (c_1, c_2), and ε = 80% (d_1, d_2) in the center and at the edge of the rod

The results of the quantitative analysis of the density of deformation microbands (ρ_{dm}) and mechanical twins (ρ_t) after *CRF* with different degrees are shown in Fig. 3. The results indicate that *CRF* leads to an increase in the density of deformation microbands, beginning at 20 % deformation (Fig. 3, *a*), and mechanical twins, beginning at 40 % deformation (Fig. 3, *b*). It should be noted that after 60 % *CRF*, the density of crystal structure defects in both cases is higher in the rod center than that at the rod edge. 80 % *CRF* causes, on the one hand, a further increase in the density of both deformation microbands and mechanical twins in the center. On the other hand, a decrease in the density of these defects occurs at the edge, apparently due to fragmentation of the microstructure during the formation of shear bands. After 80 % *CRF*, the average size of the elements of the fragmented structure at the edge of the rods of the studied steels is 200-250 nm, and in the center - 300-350 nm (Fig. 2, d_1 and d_2).

The maps of the distribution of austenite crystal orientations and the direct pole figures of the center and edge of the rod after *CRF* with different reductions are shown in Fig. 4. The direct pole figures of the rod center demonstrate a pronounced axial two-component texture <111>//rod axis *(RA)* and <100>//RA (Fig. 4, a_1-d_1), which in the subsurface layer is replaced by the simple shear texture B/B̄ (Fig. 4, a_2-d_2). It is worth noting that increasing the *CRF* reduction enhances the intensity of these texture patterns on the corresponding pole figures. A further increase in the *CRF* reduction to 80 % in the center of the rod develops the sharp axial texture <111>//RA (Fig. 4, a_1-d_1), while the fraction of austenite grains with such an orientation reaches 70 %. At the same time, after 80 % *CRF*, the volume fraction of austenite grains with
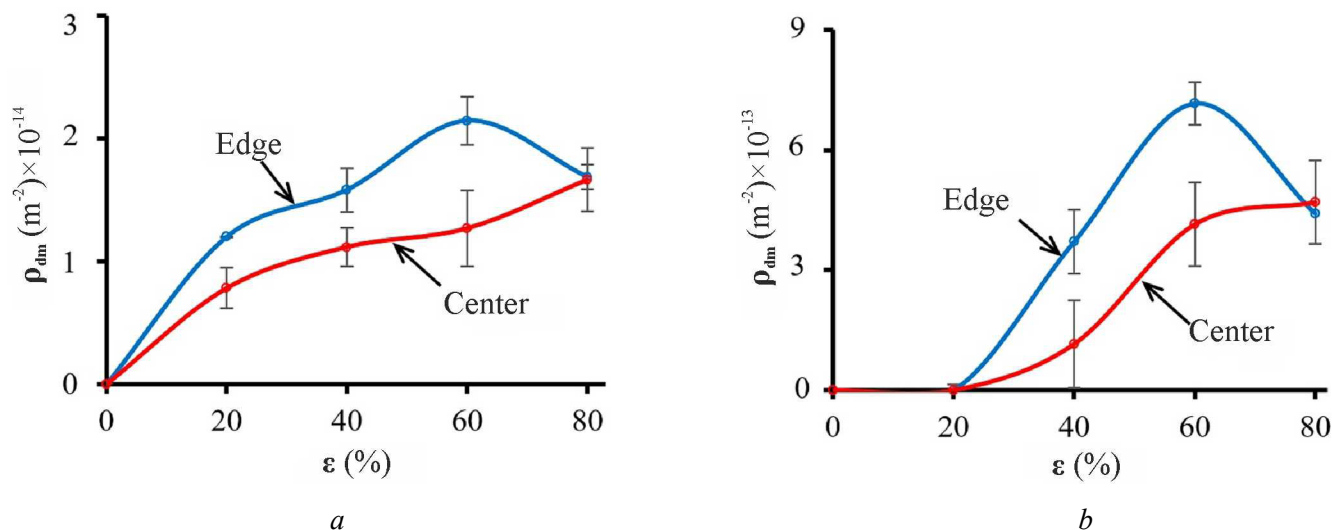
a

b

Fig. 3. Density of deformation microbands (ρ_{dm}) and mechanical twins (ρ_t) as a function of the degree of *CRF* in *Fe-21Mn-6Al-1C* steel rod at various distances from the rod center
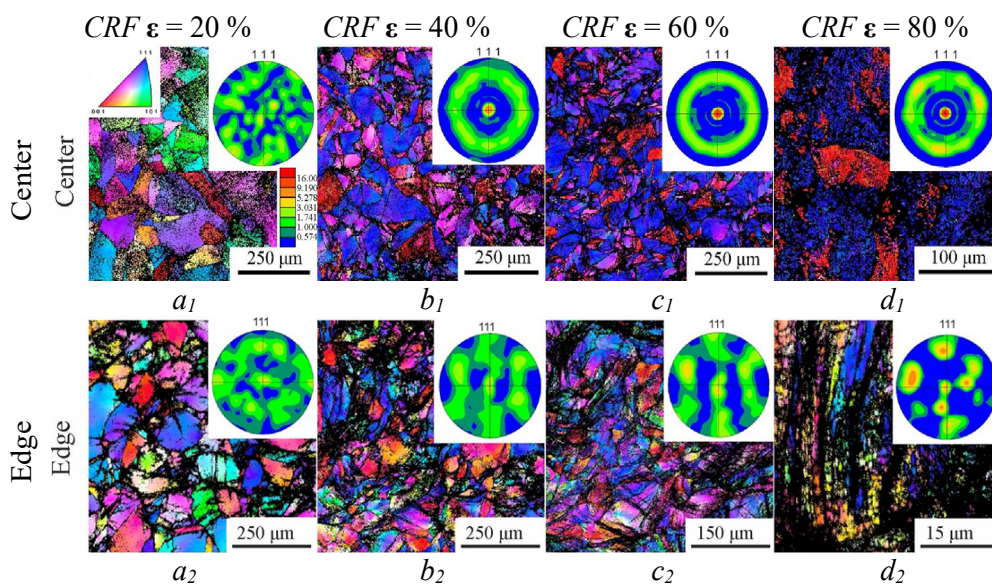

Fig. 4. Orientation maps of austenitic grains and direct pole figures (111) from the center and edge of the rod after *CRF* with $\varepsilon = 20\%$ (a_1, a_2), $\varepsilon = 40\%$ (b_1, b_2), $\varepsilon = 60\%$ (c_1, c_2), and $\varepsilon = 80\%$ (d_1, d_2)

the <100>//*RA* orientation in the center does not exceed 18 %. In this case, the fraction of austenite grains with the <111>//*RA* orientation in the direction from the center to the edge decreases to 20 %, whereas the fraction of grains with the <100>//*RA* orientation in the subsurface layer does not exceed 3 %.

The distribution of microhardness along the rod diameter depending on the degree of *CRF* of *Fe-21Mn-6Al-1C* steel is shown in Fig. 5. In the initial state, the uniform distribution of microhardness is observed over the rod cross section. The microhardness of the initial rod is at the level of 230 $HV_{0.2}$. 20 % *CRF* causes an increase in the microhardness of the rod periphery to a greater extent compared to the center, which leads to the formation of a gradient of microhardness distribution from the center to the edge of the rod. Subsequent *CRF* is accompanied by a further increase in the overall level of microhardness. However, after a deformation of 60 %, the pronounced peak of microhardness appears in the core of the rod. At the same time, in the direction from the center to the edge of the rod, the microhardness smoothly decreases, i.e. the microhardness gradient changes its direction from the edge to the center. After 80 % *CRF* this peak reaches
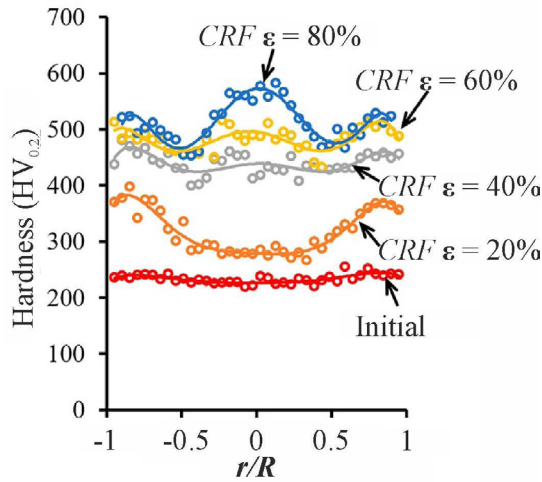
Fig. 5. Microhardness distribution in the cross-section of rods after various degrees of *CRF*

600 $HV_{0.2}$ and becomes even more pronounced. In this case, the highest overall level of microhardness is observed – 500-600 $HV_{0.2}$.

Fig. 6 and Table 1 show the tensile stress-strain diagrams and mechanical properties of *Fe-21Mn-6Al-1C* steel in the initial state (after preliminary quenching to the austenite structure) and after *CRF* with different degrees. In the initial state, the steel under study demonstrates pronounced strain hardening, as well as a high level of ductility (elongation to failure (δ) = 56-58 %; uniform elongation (δ_u) = 48-50 %) and good strength properties (ultimate tensile strength (σ_u) = 830 MPa; yield strength ($\sigma_{0.2}$) = 460 MPa).

Tensile testing of the cold-forged *Fe-21Mn-6Al-1C* steel specimens showed that the material of the center and edge of the rod demonstrates significantly different mechanical behavior (Fig. 6) and, consequently, mechanical properties (Table). Thus, the specimen cut from the center of the rod subjected to 20 % *CRF* possesses high ductility (δ = 51.4 %; δ_u = 37.9 %) along with pronounced strain hardening (Fig. 6). At
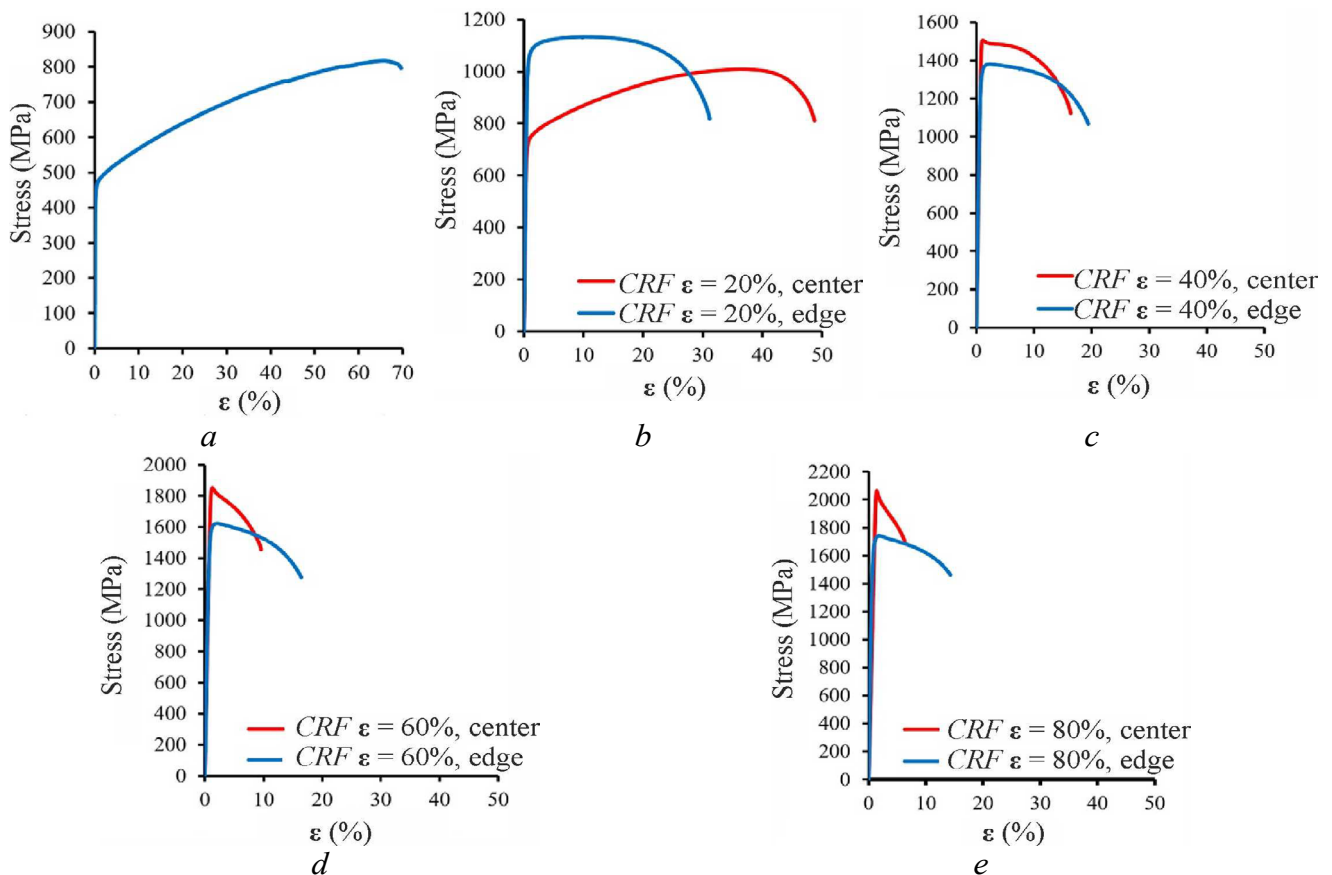

Fig. 6. Uniaxial tensile stress-strain curves of *Fe-21Mn-6Al-1C* steel in the initial state (*a*) and after *CRF* with ε = 20% (*b*), ε = 40% (*c*), ε = 60% (*d*), and ε = 80% (*e*)

Mechanical properties of *Fe-21Mn-6Al-1C* steel samples in the initial state and steel samples cut from the center and edge of rods after various *CRF* reductions

ε	0 %	20 %		40 %		60 %		80 %	
Position		Center	Edge	Center	Edge	Center	Edge	Center	Edge
σ_u, MPa	818	1,009	1,133	1,505	1,381	1,853	1,621	2,062	1,741
$\sigma_{0.2}$, MPa	459	705	1,028	1,499	1,303	1,838	1,531	2,062	1,626
δ, %	55.6	51.4	32.7	18.6	20.3	10	16.9	5.7	15.4
δ_u, %	47.9	37.9	10	0.3	1.8	0.3	1.4	0.2	1.2

the same time, an increase in the yield strength to 705 MPa and ultimate tensile strength to 1,009 MPa is observed (Table). The ductility of the edge of the rod is noticeably lower (δ = 32.7%; δ_u = 10%), while the strength characteristics are higher (σ_u = 1,133 MPa; $\sigma_{0.2}$ = 1,028 MPa). Further *CRF* is accompanied by a change in the above-mentioned ratio of strength and plasticity between the center and the edge of the rod to the opposite: the strength becomes higher at the central part of the rod, and plasticity - at the edge. For example, after 80 % *CRF*, the uniform elongation (δ_u) of the center and edge material decreases to 0.2 % and 1.2 %, respectively.

In this case, the elongation to failure of the center material is 5.7 %, and of the edge material – 15.4 %, which is mainly determined by concentrated deformation. The strength properties, in turn, of the center in the rod (σ_u = 2,062 MPa; $\sigma_{0.2}$ = 2,062 MPa) exceed these characteristics of the edge (σ_u = 1,741 MPa; $\sigma_{0.2}$ = 1,626 MPa) by 18-27 %. With an increase in the degree of *CRF*, the strain-hardening rate decreases (Fig. 7).
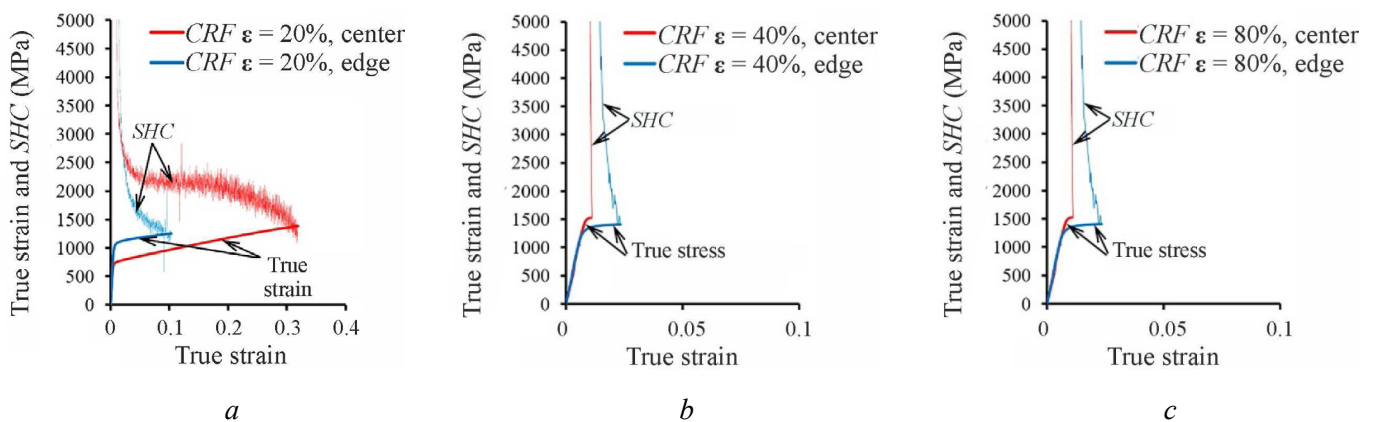

Fig. 7. True stress and strain-hardening coefficient (S*HC*) as a function of true strain during uniaxial tensile testing of samples cut from the center and edge of the rod after *CRF* with ε = 20% (*a*), ε = 40% (*b*), and ε = 80% (*c*)

Previously, using finite element modeling, it was predicted that in *CRF*, moderate tensile/compressive stresses act at the center of the rod, and high compressive stresses operate at the edge of the rod [16, 17]. Such a non-uniform stress condition leads to the accumulation of greater plastic deformation at the rod edge compared to the core. *TEM* methods have shown that in the studied steel, during *CRF*, various deformation mechanisms are activated, resulting in a whole spectrum of structural states along the rod radius. Thus, in the *Fe-21Mn-6Al-1C* steel, the following stages of microstructure formation are observed (Fig. 2): after low degrees of deformation (ε = 20 %) – formation of deformation microbands along various systems in the center and parallel deformation microbands at the rod edge; after medium degrees of deformation (ε = 40-60 %) – formation of single mechanical twins of various systems in the center and parallel packets of twins at the edge; after high degrees of deformation (ε = 80 %) – twinning according to various systems in the center and formation of a fragmented microstructure at the edge. The results of *EBSD* analysis show

that with increasing degree of *CRF*, pronounced textural gradients develop. These texture gradients are due to the fact that a sharp two-component axial texture <111>//*RA* and <100>//*RA*, is formed in the center of the rods, which weakens towards the edge. It should be noted that the shear texture B/B¯ develops at the edge of the rod after 40 % *CRF* and higher [19, 20].

The distribution of microhardness in the cross section of the rods shows the development of a gradient structure during *CRF* (Fig. 5). In the case of the initial state with a homogeneous structure, a uniform distribution of microhardness is observed across the cross-section of the rods of both steels. 20 % *CRF* is accompanied by a general increase in the hardness of the program steel. However, the hardness of the rod edge increases to a greater extent. Texture analysis showed a relatively uniform distribution of grains with <111>//*RA* and <100>//*RA* orientations across the section after 20 % *CRF,* i.e. this factor does not have a significant effect. Meanwhile, the increased density of microbands and mechanical twins is observed at the edge (Fig. 3), which is due to high strain accumulation in this place and determines an increased level of hardness. These structural changes also affect the results of uniaxial tensile tests of samples cut from the center and edge of rods of both steels. At the same time, the strength of the edge material of the rods was significantly higher than that of the material from the center (Table). Plasticity at the edge was lower mainly due to a decrease in uniform elongation due to the accumulation of a higher density of crystalline structure defects (Fig. 3).

Further 40-85 % *CRF* is accompanied by an increase in the microhardness of the rods. After 40 % *CRF*, the previously obtained microhardness gradient is smoothed out (Fig. 5). Subsequent 60-85 % *CRF* leads to the formation of the microhardness peak in the center of the studied rod. The results of the quantitative analysis of the microstructure of the studied steels showed that after 40-60 % *CRF*, an increased density of lattice defects is still observed at the edge of the rod compared to the core (Fig. 3). Additionally, a pronounced gradient of the volume fraction of austenite grains with the <111>//*RA* orientation is formed across the rod cross-section (Fig. 4). Thus, in the center of the rod, a high proportion (up to 70 %) of grains with the <111>//*RA* orientation is observed. Due to the active development of shear bands at the edge of the rod, the shear texture B/B¯ is formed. In this case, the determining factor in the occurrence of a microhardness gradient is the texture gradient, since such grains with the orientation <111>//*RA* perform a low value of the *Schmid* factor for mechanical twinning and dislocation slip (Fig. 8). The highest level of the *Schmid* factor is observed in grains with the orientation <100>//*RA*, however, the proportion of such crystals in the center of the rod does not exceed 18 %. The observed changes in the microstructure and texture during *CRF* of the studied steels to 40-85 % deformation are accompanied by a change in the ratio between the strength and ductility of the center and edge of the rod (Fig. 6). In this case, the highest strength and the lowest ductility are found in the material from the center of the rod. Following *CRF* to

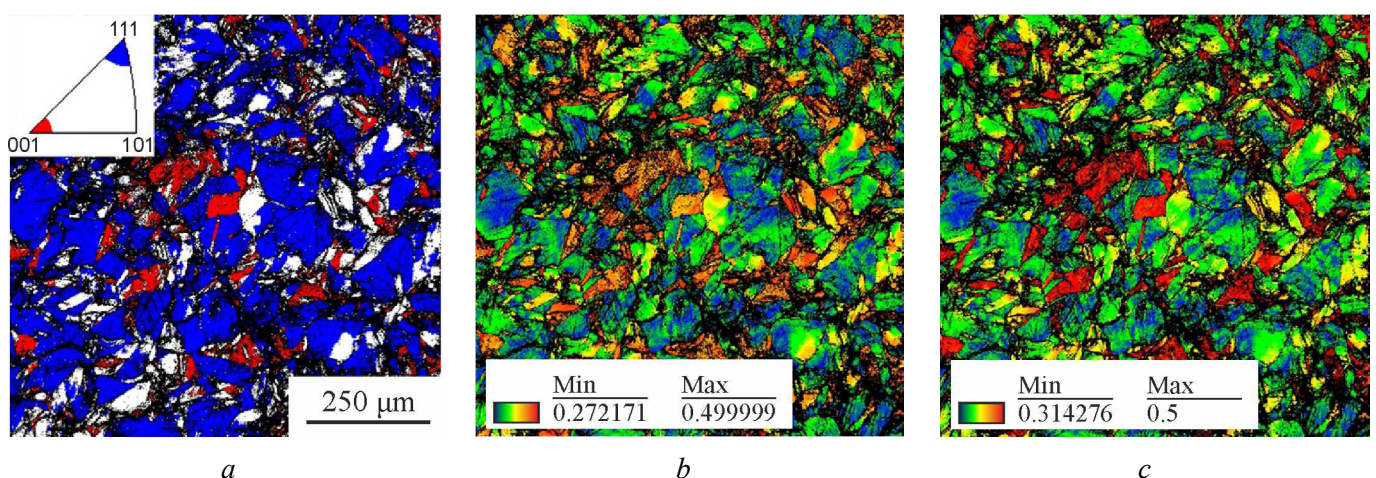*Fig. 8*. Orientation map of austenitic grains with orientations <111>//BA and <100>//BA (*a*), grain distribution based on *Schmid* factor for dislocation slip (*b*) and mechanical twinning (*c*) of *Fe-21Mn-6Al-1C* steel after *CRF* with ε = 60% in the center of the rod

60 % or higher reductions, the material from the rod center exhibits a decrease in uniform elongation to 0.2-0.3 % and a relative elongation of less than 10 % (Table). The material of the edge of the rod demonstrates a uniform elongation at the level of 1.2-1.7 %, and a relative elongation of about 14-17 %.

Conclusion

Based on the results of the study of the evolution of the microstructure, texture and mechanical properties of the lightweight austenitic steel *Fe-21Mn-6Al-1C* after various cold radial forging *(CRF)* modes, the following conclusions can be drawn:

– During *CRF*, the following stages of the microstructure formation are observed: low degrees of deformation (ε up to 20 %) – formation of deformation microbands of various systems in the center and parallel deformation microbands at the edge of the rod; medium degrees of deformation (ε = 40-60 %) – formation of single mechanical twins of various systems in the center and parallel packets of twins at the edge; high degrees of deformation (ε = 80 %) – twinning according to various systems in the center and formation of a fragmented microstructure at the edge.

– With an increase in the degree of *CRF*, pronounced texture gradients are formed in the rod. The two-component axial texture <111>// rod axis *(RA)* and <100>//*RA* develops in the center of the rod, which is weakened towards the edge. Meanwhile, the pronounced shear texture B/B¯ is found at the edge of the rod after 40 % *CRF* and higher.

– 20 % *CRF* causes an increase in microhardness of the rod edge to a greater extent compared to the center. Subsequent *CRF* is accompanied by a further increase in the overall level of microhardness. After a deformation of 60%, a pronounced peak of microhardness appears in the core of the rod. After 80 % *CRF*, this peak reaches 600 $HV_{0.2}$.

– After 20 % *CRF*, the material of the rod center exhibits higher strength and lower ductility compared to the material of the rod edge. With further *CRF*, the strength becomes higher at the center of the rod, whereas the ductility is higher at the edge. Thus, after 80 % *CRF*, elongation to failure is $\boldsymbol{\delta} \approx 6$ % at the center and $\boldsymbol{\delta} \approx 15$ % at the edge. The strength properties of the central part of the rod ($\boldsymbol{\sigma_u}$ = ,2062 MPa; $\boldsymbol{\sigma_{0.2}}$ = 2,062 MPa) exceed these characteristics of the edge ($\boldsymbol{\sigma_u}$ = 1,741 MPa; $\boldsymbol{\sigma_{0.2}}$ = 1,626 MPa) by 20-30 %.

References

1. Chen S., Rana R., Haldar A., Ray R.K. Current state of Fe-Mn-Al-C low density steels. *Progress in Materials Science*, 2017, vol. 89, pp. 345–391. DOI: 10.1016/j.pmatsci.2017.05.002.

2. Raabe D., Springer H., Gutierrez-Urrutia I., Roters F., Bausch M., Seol J.B., Koyama M., Choi P.P., Tsuzaki K. Alloy design, combinatorial synthesis, and microstructure–property relations for low-density Fe-Mn-Al-C austenitic steels. *Jom*, 2014, vol. 66, pp. 1845–1856. DOI: 10.1007/s11837-014-1032-x.

3. Ding H., Liu D., Cai M., Zhang Y. Austenite-based Fe-Mn-Al-C lightweight steels: research and prospective. *Metals*, 2022, vol. 12 (10), p. 1572. DOI: 10.3390/met12101572.

4. Kim H., Suh D., Kim N.J., Kim H., Suh D., Kim N.J. Fe–Al–Mn–C lightweight structural alloys: a review on the microstructures and mechanical properties. *Science and Technology of Advanced Materials*, 2013, vol. 14 (1), p. 014205. DOI: 10.1088/1468-6996/14/1/014205.

5. Yoo J.D., Hwang S.W., Park K.T. Origin of extended tensile ductility of a Fe-28Mn-10Al-1C steel. *Metallurgical and Materials Transactions: A*, 2009, vol. 40 (7), pp. 1520–1523. DOI: 10.1007/s11661-009-9862-9.

6. Moon J., Park S.J., Jang J.H., Lee T.H., Lee C.H., Hong H.U., Han H.N., Lee J., Lee B.H., Lee C. Investigations of the microstructure evolution and tensile deformation behavior of austenitic Fe-Mn-Al-C lightweight steels and the effect of Mo addition. *Acta Materialia*, 2018, vol. 147, pp. 226–235. DOI: 10.1016/j.actamat.2018.01.051.

7. Chen P., Zhang F., Zhang Q.C., Du J.H., Shi F., Li X.W. Precipitation behavior of κ-carbides and its relationship with mechanical properties of Fe–Mn–Al–C lightweight austenitic steel. *Journal of Materials Research and Technology*, 2023, vol. 25 (12), pp. 3780–3788. DOI: 10.1016/j.jmrt.2023.06.212.

8. Harwarth M., Chen G., Rahimi R., Biermann H., Zargaran A., Duffy M., Zupan M., Mola J. Aluminum-alloyed lightweight stainless steels strengthened by B2-(Ni,Fe)Al precipitates. *Materials & Design*, 2021, vol. 206, p. 109813. DOI: 10.1016/j.matdes.2021.109813.

9. Kim C.W., Kwon S.I., Lee B.H., Moon J.O., Park S.J., Lee J.H., Hong H.U. Atomistic study of nano-sized κ-carbide formation and its interaction with dislocations in a cast Si added FeMnAlC lightweight steel. *Materials Science and Engineering: A*, 2016, vol. 673, pp. 108–113. DOI: 10.1016/j.msea.2016.07.029.

10. Li Z., Wang Y.C., Cheng X., Gao C., Li Z., Langdon T.G. Microstructure and mechanical properties of an Fe–Mn–Al–C lightweight steel after dynamic plastic deformation processing and subsequent aging. *Materials Science and Engineering: A*, 2022, vol. 833, p. 142566. DOI: 10.1016/j.msea.2021.142566.

11. Rahnama A., Kotadia H., Sridhar S. Effect of Ni alloying on the microstructural evolution and mechanical properties of two duplex light-weight steels during different annealing temperatures: experiment and phase-field simulation. *Acta Materialia*, 2017, vol. 132 (6), pp. 627–643. DOI: 10.1016/j.actamat.2017.03.043.

12. Xiang S., Liu X., Xu R., Yin F., Cheng G.J. Ultrahigh strength in lightweight steel via avalanche multiplication of intermetallic phases and dislocation. *Acta Materialia*, 2023, vol. 242, p. 118436. DOI: 10.1016/j.actamat.2022.118436.

13. Moon J., Park S.J., Lee C.H., Hong H.U., Lee B.H., Kim S.D. Influence of microstructure evolution on hot ductility behavior of austenitic Fe–Mn–Al–C lightweight steels during hot tensile deformation. *Materials Science and Engineering: A*, 2023, vol. 868, p. 144786. DOI: 10.1016/j.msea.2023.144786.

14. Mao Q., Liu Y., Zhao Y. A review on mechanical properties and microstructure of ultrafine grained metals and alloys processed by rotary swaging. *Journal of Alloys and Compounds*, 2022, vol. 896, p. 163122. DOI: 10.1016/j.jallcom.2021.163122.

15. Macháčková A., Krátká L., Petrmichl R., Kuncická L., Kocich R. Affecting structure characteristics of rotary swaged tungsten heavy alloy via variable deformation temperature. *Materials*, 2019, vol. 12 (24), p. 4200. DOI: 10.3390/ma12244200.

16. Panov D., Chernichenko R., Kudryavtsev E., Klimenko D., Naumov S., Pertcev A. Effect of cold swaging on the bulk gradient structure formation and mechanical properties of a 316-type austenitic stainless steel. *Materials*, 2022, vol. 15 (7), p. 2468. DOI: 10.3390/ma15072468.

17. Panov D., Kudryavtsev E., Naumov S., Klimenko D., Chernichenko R., Mirontsov V., Stepanov N., Zherebtsov S., Salishchev G., Pertcev A. Gradient microstructure and texture formation in a metastable austenitic stainless steel during cold rotary swaging. *Materials*, 2023, vol. 16 (4), p. 1706. DOI: 10.3390/ma16041706.

18. Panov D.O., Kudryavtsev E.A., Chernichenko R.S., Naumov S.V., Klimenko D.N., Stepanov N.D., Zherebtsov S.V., Salishchev G.A., Sanin V.V., Pertsev A.S. Excellent strength-ductility combination of interstitial non-equiatomic middle-entropy alloy subjected to cold rotary swaging and post-deformation annealing. *Materials Science and Engineering: A*, 2024, vol. 898, p. 146121. DOI: 10.1016/j.msea.2024.146121.

19. Fonda R.W., Knipling K.E. Texture development in friction stir welds. *Science and Technology of Welding & Joining*, 2011, vol. 16 (4), pp. 288–294. DOI: 10.1179/1362171811Y.0000000010.

20. Suwas S., Ray R.K. *Crystallographic texture of materials.* London, Springer, 2014. 265 p. ISBN 978-1-4471-6313-8. DOI: 10.1007/978-1-4471-6314-5.

Conflicts of Interest

The authors declare no conflict of interest.